THE ASTROPHYSICAL JOURNAL, 565:405–412, 2002 January 20

EXPLOSIVE NUCLEOSYNTHESIS IN ASPHERICAL HYPERNOVA EXPLOSIONS AND LATE-TIME SPECTRA OF SN 1998bw

KEIICHI MAEDA,[1] TAKAYOSHI NAKAMURA,[1] KEN'ICHI NOMOTO,[1,2] PAOLO A. MAZZALI,[2,3]
FERDINANDO PATAT,[4] AND IZUMI HACHISU[5]
Received 2000 October 10; accepted 2001 September 19

ABSTRACT

Aspherical explosion models for the hypernova (hyperenergetic supernova) SN 1998bw are presented. Nucleosynthesis in aspherical explosions is examined with a two-dimensional hydrodynamical code and a detailed nuclear reaction network. Aspherical explosions lead to a strong α-rich freezeout, thus enhancing the abundance ratios [^{44}Ca, ^{48}Ti, ^{64}Zn/Fe] in the ejecta. The nebular line profiles of the Fe-dominated blend near 5200 Å and of [O I] 6300, 6363 Å are calculated and compared with the observed late-time spectra of SN 1998bw. Compared with the spherical model, the unusual features of the observed nebular spectra can be better explained if SN 1998bw is a strongly aspherical explosion with a kinetic energy of $\sim 10^{52}$ ergs viewed from near the jet direction.

Subject headings: gamma rays: bursts — line: profiles — nuclear reactions, nucleosynthesis, abundances — supernovae: individual (SN 1998bw)

1. INTRODUCTION

The exceptionally bright Type Ic supernova (SN Ic) SN 1998bw was discovered as the probable optical counterpart of the γ-ray burst GRB 980425 (Galama et al. 1998). The early light curve and the spectra of SN 1998bw have been successfully modeled as the hyperenergetic explosion (kinetic energy $E \sim 4 \times 10^{52}$ ergs) of a massive C+O star (Iwamoto et al. 1998; Woosley, Eastman, & Schmidt 1999; Branch 2001). In this paper the term "hypernova" is used to refer to a SN explosion with $E \gtrsim 10^{52}$ ergs, regardless of the nature of the central engine (Nomoto et al. 2001a).

Despite the success of the hypernova model in reproducing the observed features of SN 1998bw at early times, some properties of the observed light curve and spectra at late times are difficult to explain. (1) The tail of the observed light curve declines more slowly than the synthetic curve, indicating that at advanced epochs γ-ray trapping is more efficient than expected (Nakamura et al. 2001a; Sollerman et al. 2000). (2) In the nebular epoch, the [O I] 6300 Å emission is narrower than the emission near 5200 Å. As discussed in Mazzali et al. (2001), this latter feature is mostly due to a blend of [Fe II] lines. Mazzali et al. (2001) calculated synthetic nebular phase spectra of SN 1998bw using a spherically symmetric non-LTE nebular code based on the deposition of γ-rays from ^{56}Co decay in a nebula of uniform density and composition. They showed that the [O I] and the [Fe II] features can be reproduced only if different velocities are assumed for the two elements. A significant amount of slowly moving O is therefore necessary to explain the profile of the [O I] line.

Both these features are in conflict with what is expected from a spherically symmetric explosion model, where γ-ray deposition decreases with time and where iron is produced in the deepest layers and thus has a lower average velocity than oxygen. Mazzali et al. (2001) suggested that these are signatures of asymmetry in the ejecta. Therefore, in this paper we examine aspherical explosion models for hypernovae.

Aspherical explosions of massive stars have been investigated as possible sources of γ-ray bursts (Woosley 1993; Paczyński 1998). MacFadyen & Woosley (1999) showed numerically that the collapse of a rotating massive core can form a black hole with an accretion disk while a jet emerges along the rotation axis. The jet produces a highly asymmetric explosion (Khokhlov et al. 1999). However, these studies did not calculate explosive nucleosynthesis, nor did they show spectroscopic and photometric features of aspherical explosions. Nagataki (2000) performed nucleosynthesis calculations for aspherical SN explosions to explain some features of SN 1987A, but he only addressed the case of a normal explosion energy.

In the present study, we examine the effect of aspherical explosions on nucleosynthesis in hypernovae. We then investigate the degree of asphericity in the ejecta of SN 1998bw, which is critically important information to confirm the SN/GRB connection, by computing synthetic spectra for the various models viewed with different orientations and comparing the results with the observed late-time spectra of SN 1998bw (Patat et al. 2001).

2. ASYMMETRIC EXPLOSION MODELS

The first step of our calculation is the hydrodynamical simulation of the explosion with a two-dimensional Eulerian hydrodynamical code based on Roe's scheme (Hachisu et al. 1992, 1994). Euler's equations are solved with a constant adiabatic index of $\gamma = 4/3$, which is a good approximation if the pressure is radiation dominated. The effect of nuclear reactions on the hydrodynamics is negligible since the explosion energy is large. We use 120×120 meshes on a cylindrical (r, z) coordinate system. The mesh size is linearly zoned and decreases inward, which gives a high resolution of the hydrodynamic evolution of the

[1] Department of Astronomy, School of Science, University of Tokyo, Bunkyo-ku, Tokyo 113-0033, Japan; maeda@astron.s.u-tokyo.ac.jp, nakamura@astron.s.u-tokyo.ac.jp.
[2] Research Center for the Early Universe, School of Science, University of Tokyo, Bunkyo-ku, Tokyo 113-0033, Japan; nomoto@astron.s.u-tokyo.ac.jp, mazzali@ts.astro.it.
[3] Osservatorio Astronomico di Trieste, via G. B. Tiepolo 11, I-34131 Trieste, Italy.
[4] European Southern Observatory, Karl-Schwarzschild-Strasse 2, D-85748 Garching, Germany; fpatat@eso.org.
[5] Department of Earth Science and Astronomy, College of Arts and Science, University of Tokyo, Meguro-ku, Tokyo 153-0041, Japan; hachisu@chianti.c.u-tokyo.ac.jp.

central regions where explosive nucleosynthesis takes place. We follow 190 test particles initially in the Si layer and 2250 particles initially in the C+O layer, tracking their density and temperature histories. These histories are then used to calculate the change in the chemical composition, using a reaction network including 222 isotopes up to ^{71}Ge (Thielemann, Nomoto, & Hashimoto 1996).

We construct several asymmetric explosion models for various combinations of the model parameters (Table 3). We use as progenitor the 16 $M_\odot$ He core of a 40 $M_\odot$ star (Nomoto & Hashimoto 1988). This has a 13.8 $M_\odot$ C+O core, the same as that used in Iwamoto et al. (1998). We test three values of the final kinetic energy: $E = 1 \times 10^{51}$, 1×10^{52}, and 3×10^{52} ergs. The hydrodynamical simulation is started by depositing the energy below the mass cut that divides the ejecta from the collapsing core. The energy deposited is divided between thermal and kinetic energy, with various ratios. The asymmetry is generated by distributing the initial kinetic energy in an axisymmetric way. This is done by imposing different initial velocities in different directions: $v_z = \alpha z$ in the jet direction and $v_r = \beta r$ on the equatorial plane. The ratio α/β ranges from 16:1 to 1:1 (spherical case). The mass cut is set at $M_r = 2.4\ M_\odot$ so that the ejected mass of ^{56}Ni is $\sim 0.4\ M_\odot$ to reproduce the peak of the light curve (Nakamura et al. 2001a) in models A, B, C, E, and F.

3. NUCLEOSYNTHESIS

Figures 1 and 2 show, respectively, the postshock peak temperatures and densities for the asymmetric hypernova model C in the direction of the jet and perpendicular to it (with those for the spherically symmetric hypernova model F also shown for comparison) and the isotopic composition of the ejecta of model C. In the z-direction, where the ejecta carry more kinetic energy, the shock is stronger and postshock temperatures are higher so that explosive nucleosynthesis takes place in more extended, lower density regions compared with the r-direction. Therefore, larger amounts of α-rich freezeout elements, such as ^{4}He and ^{56}Ni (which decays into ^{56}Fe via ^{56}Co), are produced in the z-direction than in the r-direction. Also, the expansion velocity of newly synthesized heavy elements is much higher in the z-direction. The velocity of elements ejected in the z-direction in model C is actually similar to the result of a spherical explosion with $E \sim 3 \times 10^{52}$ ergs (Nakamura et al. 2001b), although the integrated kinetic energy is only $E = 1 \times 10^{52}$ ergs.

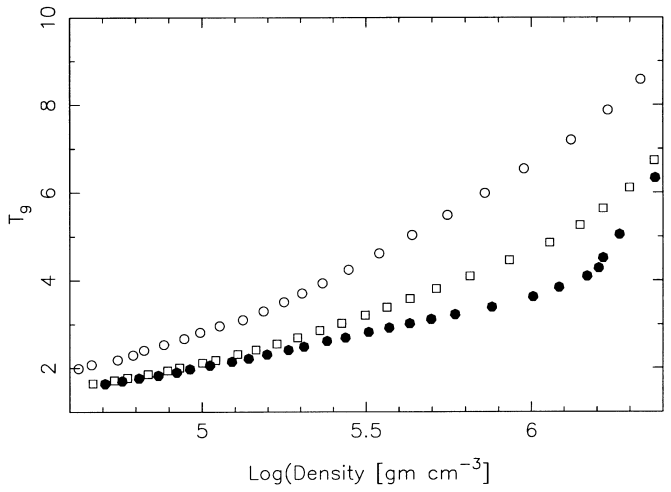

FIG. 1.—The ρ-T conditions of individual test particles at their temperature maximum [where $T_9 \equiv T(\mathrm{K})/10^9$]. For model C, open circles denote those along the z-axis and filled circles denote those along the r-axis. Open squares denote those of model F (spherical model).

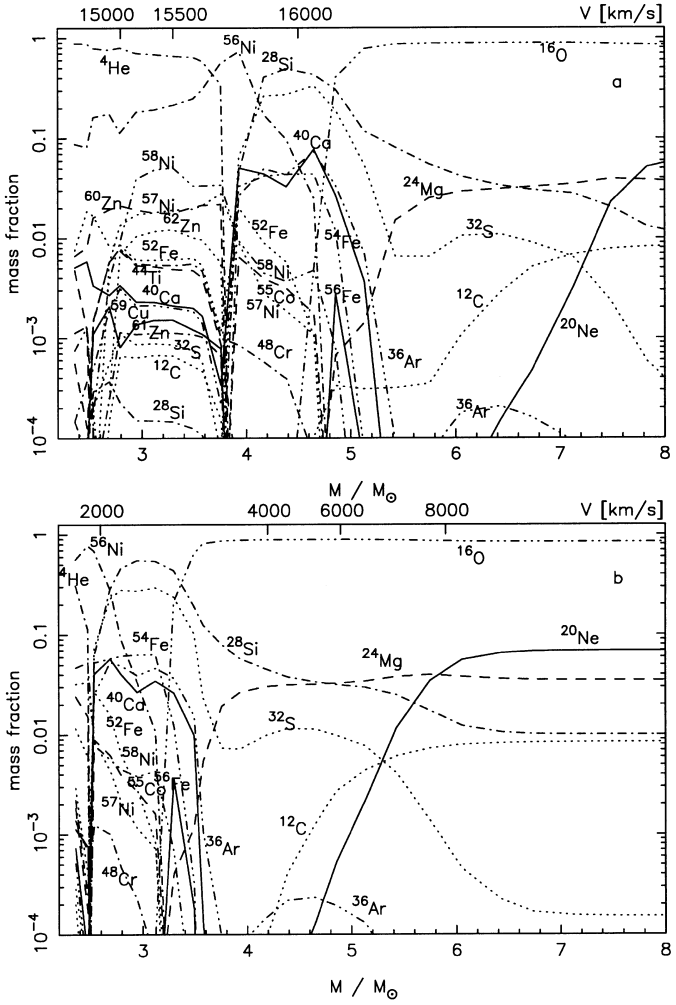

FIG. 2.—Isotopic composition of the ejecta of model C in the direction of the jet (*upper panel*) and perpendicular to the jet (*lower panel*). The ordinate indicates the initial spherical Lagrangian coordinate (M_r) of the test particles (*lower scale*), and the final expansion velocities (V) of those particles (*upper scale*).

In contrast, along the r-direction ^{56}Ni is produced in only the deepest layers, and elements ejected in this direction are mostly the product of hydrostatic nuclear burning (O), with some explosive oxygen-burning products (e.g., Si, S). The expansion velocities are much lower than in the z-direction.

Figure 3 shows the two-dimensional distribution of ^{56}Ni and ^{16}O in model C in the homologous expansion phase. Near the z-axis the shock is stronger, and a low-density ^{4}He-rich region is produced. ^{56}Ni is distributed preferentially in this direction, but it is mostly located slightly off of it because the shock propagates laterally as it penetrates the stellar envelope. As a result, the distribution of heavy elements is elongated in the z-direction while that of ^{16}O is less aspherical. On the other hand, because the ejecta moves more slowly in the r-direction, densities in this direction are higher than in the z-direction.

Tables 1 and 2 give, respectively, the detailed yields and the abundances of major stable isotopes relative to the solar

TABLE 1

DETAILED YIELDS OF MODEL C

Species	Yield ($M_\odot$)	Species	Yield ($M_\odot$)	Species	Yield ($M_\odot$)	Species	Yield ($M_\odot$)	Species	Yield ($M_\odot$)
^{12}C	1.35E−01	^{13}C	1.84E−08	^{14}N	8.13E−05	^{15}N	2.63E−08	^{16}O	8.72
^{17}O	1.11E−07	^{18}O	1.77E−06	^{19}F	1.45E−09	^{20}Ne	5.38E−01	^{21}Ne	1.92E−03
^{22}Ne	5.51E−02	^{23}Na	1.87E−02	^{24}Mg	3.35E−01	^{25}Mg	4.08E−02	^{26}Mg	8.86E−02
^{26}Al	6.28E−05	^{27}Al	7.06E−02	^{28}Si	5.27E−01	^{29}Si	5.43E−02	^{30}Si	5.65E−02
^{31}P	7.09E−03	^{32}S	2.37E−01	^{33}S	9.40E−04	^{34}S	1.45E−02	^{36}S	1.71E−05
^{35}Cl	3.92E−04	^{37}Cl	8.90E−05	^{36}Ar	4.01E−02	^{38}Ar	5.73E−03	^{40}Ar	1.98E−07
^{39}K	3.31E−04	^{40}K	7.56E−08	^{41}K	2.30E−05	^{40}Ca	3.57E−02	^{42}Ca	1.67E−04
^{43}Ca	1.25E−05	^{44}Ca	1.62E−03	^{46}Ca	1.23E−09	^{45}Sc	2.39E−06	^{46}Ti	6.93E−05
^{47}Ti	5.57E−05	^{48}Ti	2.02E−03	^{49}Ti	3.90E−05	^{50}Ti	1.36E−09	^{50}V	4.60E−09
^{51}V	9.91E−05	^{50}Cr	4.39E−04	^{52}Cr	8.25E−03	^{53}Cr	7.72E−04	^{54}Cr	1.52E−07
^{55}Mn	3.00E−03	^{54}Fe	3.87E−02	^{56}Fe	3.95E−01	^{57}Fe	1.65E−02	^{58}Fe	4.88E−08
^{59}Co	6.56E−04	^{58}Ni	2.71E−02	^{60}Ni	1.20E−02	^{61}Ni	6.09E−04	^{62}Ni	5.08E−03
^{64}Ni	4.29E−12	^{63}Cu	1.80E−05	^{65}Cu	1.12E−05	^{64}Zn	1.60E−04	^{66}Zn	8.93E−05
^{67}Zn	6.53E−07	^{68}Zn	1.23E−07	^{69}Ga	9.72E−10	^{71}Ga	2.45E−10	^{70}Ge	1.02E−09

values for model C (in Table 2, $[A/B] \equiv \log_{10}(A/B) - \log_{10}(A/B)_\odot$, where A and B are nuclear mass fractions). The main characteristics can be summarized as follows (see also Nomoto et al. 2001b):

1. The complete Si-burning region is more extended for larger explosion energies. The aspherical explosion causes a region of higher entropy along the z-axis, which offers better conditions for the α-rich freezeout (Fig. 1). The high entropy inhibits the production of ^{56}Ni. Much ^{4}He is left after the freezeout, so the elements produced through ^{4}He capture are very abundant in the deepest region along the z-axis (Fig. 2). This results in the enhancement of the elements synthesized in the deepest region, such as ^{44}Ca (produced as ^{44}Ti), ^{48}Ti (as ^{48}Cr), and elements heavier than $A \sim 58$.

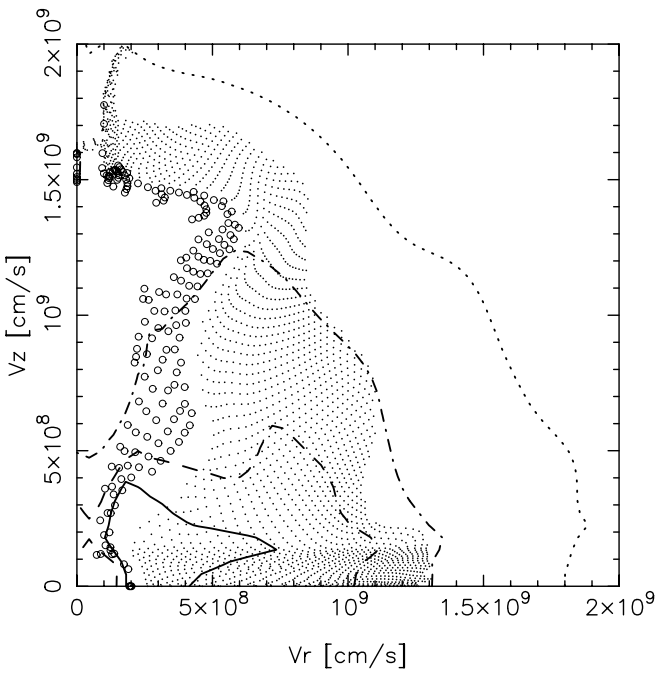

FIG. 3.—Two-dimensional distribution of ^{56}Ni (*open circles*) and ^{16}O (*dots*) of model C in the homologous expansion phase. Open circles and dots denote test particles in which the mass fractions of ^{56}Ni and ^{16}O, respectively, exceeds 0.1. Lines are density contours at the level of 0.5 (*solid lines*), 0.3 (*dashed lines*), 0.1 (*dash-dotted lines*), and 0.01 (*dotted lines*) of the maximum density.

Because of the enhancement of these elements and the simultaneous suppression of ^{56}Ni, the abundances of these elements relative to iron (e.g., [^{44}Ca, ^{48}Ti, ^{64}Zn/Fe]) are greatly enhanced. For more asymmetric explosion, the effect of α-rich freezeout is even larger.

2. Incomplete Si-burning and O-burning regions are more extended for larger explosion energies (Nakamura et al. 2001b). This results in the enhancement of ^{28}Si, ^{32}S, ^{40}Ca, ^{52}Cr (produced as ^{52}Fe) and ^{54}Fe and in the reduction of O. Asphericity has little effect on the production of these elements.

The most pronounced effect of asphericity is that elements produced by the strong α-rich freezeout are greatly enhanced relative to iron (e.g., [Ti/Fe]). For other explosive burning products, the effect of a large explosion energy usually dominates over that of asphericity.

4. THE LATE-TIME SPECTRA OF SN 1998bw

In order to verify the observable consequences of an axisymmetric explosion, we calculated the profiles of the [Fe II] blend and of [O I] for models A–G. Line emissivities were obtained from a one-dimensional non-LTE nebular

TABLE 2

ABUNDANCES OF MAJOR STABLE ISOTOPES RELATIVE TO THE SOLAR VALUES FOR MODEL C

Species	[X/O][a]	[X/Fe]	Species	[X/O]	[X/Fe]
^{12}C	−1.31	−0.880	^{40}Ca	−0.183	0.246
^{14}N	−4.09	−3.66	^{44}Ca	0.0989	0.529
^{16}O	0.000	0.430	^{45}Sc	−1.17	−0.740
^{19}F	−5.40	−4.97	^{48}Ti	0.0153	0.445
^{20}Ne	−0.437	−0.00731	^{51}V	−0.538	−0.109
^{23}Na	−0.210	0.220	^{52}Cr	−0.215	0.215
^{24}Mg	−0.146	0.284	^{55}Mn	−0.605	−0.176
^{27}Al	0.127	0.557	^{54}Fe	−0.224	0.206
^{28}Si	−0.0516	0.378	^{56}Fe	−0.430	0.000
^{31}P	−0.0192	0.411	^{59}Co	−0.668	−0.238
^{32}S	−0.182	0.248	^{58}Ni	−0.220	0.210
^{35}Cl	−0.769	−0.339	^{63}Cu	−1.46	−1.03
^{36}Ar	−0.244	0.186	^{64}Zn	−0.750	−0.320
^{39}K	−0.979	−0.549			

[a] $[A/B] \equiv \log_{10}(A/B) - \log_{10}(A/B)_\odot$

code (Mazzali et al. 2001), and the column densities of the various elements along different lines of sight were derived from the element distribution obtained from our two-dimensional explosion models. Because we assume that the nebula is optically thin, the blended nature of the emissions is automatically taken into account.

These are compared to the 1998 November 26 spectrum of SN 1998bw. We select this spectrum because the wavelength of the 5200 Å feature, which was somewhat redder at earlier epochs, at this and later epochs coincides with that of the equivalent [Fe II] feature in the nebular spectra of SNe Ia (Axelrod 1980), indicating that other contributions (see § 5) are now negligible. Table 3 gives the FWHM of our synthetic lines as a function of viewing angle. The corresponding observed value is 380 Å for the Fe blend. This is estimated assuming that the continuum level is the value around 5700 Å where the flux has the minimum value.

The FWHM of the 5200 Å feature is narrower at this epoch than at earlier ones as is that of [O I]. While for the former feature other contributions may be responsible for a broader line at earlier epochs, in the case of [O I] the decreasing density of the outer envelope must be the principal reason. At late epochs the density of the outer envelope is expected to be too small to trap the γ-rays. Therefore, we set the outermost velocity of the emitting region to reproduce the FWHM of the [O I] line (150 Å) and then calculate the profiles of the [Fe II] blend.

The [Fe II] and [O I] profiles for model C viewed at an angle of 15° from the jet direction and those for model F are compared to the observed spectrum of 1998 November 26 in Figure 4. For model F in Figure 4, the outermost velocity of the emitting region is set to make the [Fe II] line as broad as possible because for this model we cannot get a reasonable fit for the [O I] line, which is always much broader than the observation. Indeed, fitting the [O I] line was not possible for all models. Among the hypernova models, in a spherical explosion (model F) oxygen is located at higher velocities than iron, and the [O I] line is too broad for any choice of the outer velocity of the emitting region. This is due to the deficiency of oxygen with small velocity along the line of sight. Also, even though the Fe feature can be wider than the O line if O and Fe are mixed extensively, the expected ratio of the width of the Fe blend and the O line even in a fully mixed model is $\sim 3:2$ (Mazzali et al. 2001). This is the result of taking blending into account but giving all contributing lines the same intrinsic width. However, the observed ratio is even larger, $\gtrsim 2:1$, implying that the [Fe II] lines are intrinsically broader than the [O I] line. Therefore, the observed line profiles are not explained with a spherical hypernova model. The same is true for the moderately asymmetric model E viewed near the equator.

In our aspherical explosion models Fe is distributed preferentially along the jet direction, and so a larger ratio of the Fe and O line widths can be obtained. All the strongly

TABLE 3

HALF-LINE WIDTHS

Model	α/β	$E/10^{51}$ergs	E_K fraction[a]	Angle[b] (deg)	Fe FWHM[c] (Å)	O FWHM (Å)	Outer Velocity (km s^{-1})
A.....	16	10	0.65	5	376	150	9000
				15	344	150	8500
				30	304	150	8000
				45	248	150	6500
				60	216	150	5000
				75	144	150	4500
				85	144	150	4500
B.....	8	30	0.5	5	352	150	10000
				15	344	150	9500
				>30	...	Too broad [O I]	...
C.....	8	10	0.5	5	296	150	10000
				15	304	150	9500
				30	280	150	8500
				45	232	150	6500
				60	216	150	5000
				75	176	150	4500
				85	160	150	4000
D.....	8	1	0.5	5	224	80	5000
				15	216	80	5000
				30	216	72	5000
				45	200	80	5000
				60	192	80	5000
				75	160	88	5000
				85	128	88	5000
E.....	2	10	0.5	5	288	150	8500
				15	296	150	8000
				30	264	150	7000
				>45	...	Too broad [O I]	...
F.....	1	10	0.5	...	...	Too broad [O I]	...
G.....	1	1	0.5	...	144	96	3500

[a] The ratio of the kinetic energy to E initially deposited.
[b] Angle between the line of sight and the jet direction.
[c] Half-line widths of the [Fe II] blend (near 5200 Å) for SN 1998bw. The observed value is 380 Å.

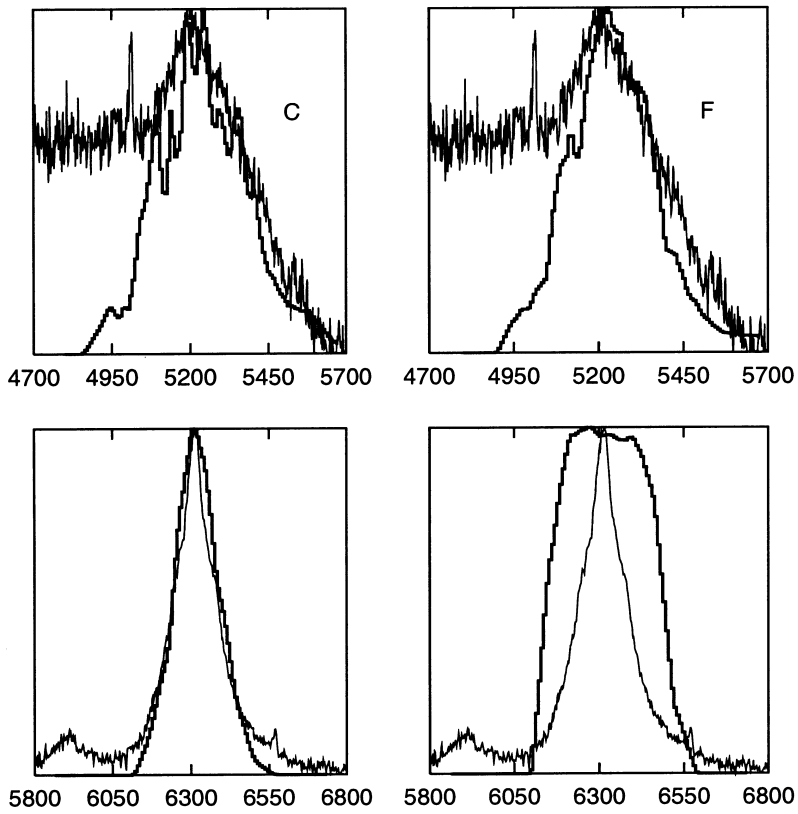

FIG. 4.—Profiles of the [Fe II] feature (*upper panels*) and of [O I] 6300, 6363 Å (*lower panels*) for model C viewed at 15° from the jet direction (*left panels*: *thick lines*) and for model F (*right panels*). Observed lines at a SN rest-frame epoch of 216 days are also plotted for comparison (*thin lines*; Patat et al. 2001). The intensities of the strongest lines, normalized to O I] λ6300.3 are [Fe II] λ5158.8: 0.122, [Fe II] λ5220.1: 0.026, [Fe II] λ5261.6: 0.083, [Fe II] λ5273.3: 0.039, [Fe II] λ5333.6: 0.060, [Fe III] λ5270.4: 0.032, [O I] λ5577.3: 0.022, and [O I] λ6363.8: 0.330.

aspherical hypernova models A, B, and C, when viewed from a near-jet direction, give line widths comparable to the observed values. The very energetic model B cannot reproduce the O line when viewed near the equator, but this is because O is too fast near the equator and too depleted near the poles to give a low-velocity component.

When the degree of asphericity is high and the explosion is viewed from near the jet direction, the component lines in the [Fe II] blend have double-peaked profiles, the blue- and redshifted peaks corresponding to matter situated in the two opposite lobes of the jet, where Fe is mostly produced. Because of the high velocity of Fe, the peaks are widely separated and the blend is wide (Fig. 4; model C). In contrast, the [O I] line is narrower and has a sharper peak because O is produced mostly in the *r*-direction, at lower velocities and with a less aspherical distribution.

Figure 5 shows the [O I] line for model C at different orientations. The mean expansion velocity of O is lower in the aspherical cases than in the spherical model because in aspherical models low-velocity, high-density, O-dominated matter is found near the center (Fig. 3). Therefore, the width of the O line in the aspherical models (A, C) viewed from near the equator can also be comparable to the observed width. This, however, does not mean that the line profile is always sharp as is seen in SN 1998bw. As shown in Figure 5, when the angle is large, the line first broadens then eventually it develops two peaks. The reason can be seen in Figure 3. The highest density region has a typical velocity of

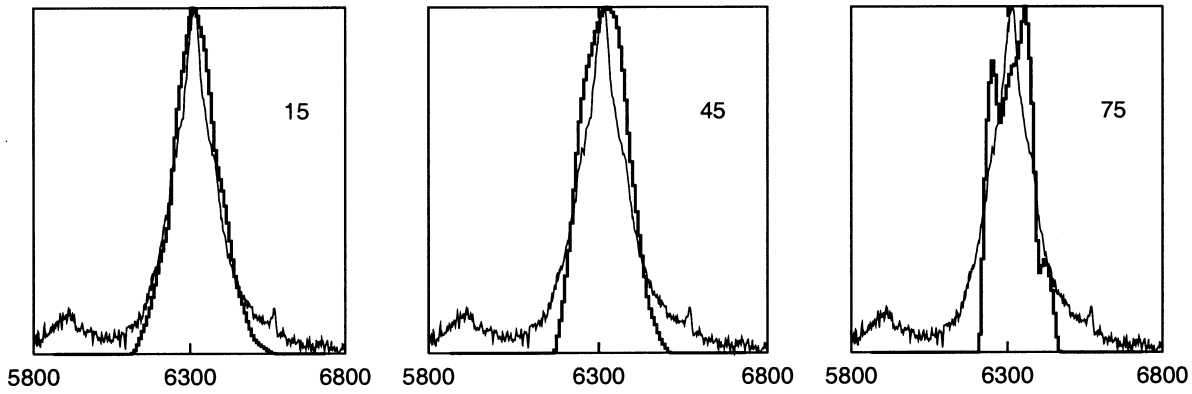

FIG. 5.—Profiles of [O I] λλ6300, 6363 for model C with different orientations. The angles between the observer and the *z*-axis are 15° (*left panel*), 45° (*middle panel*), and 75° (*right panel*).

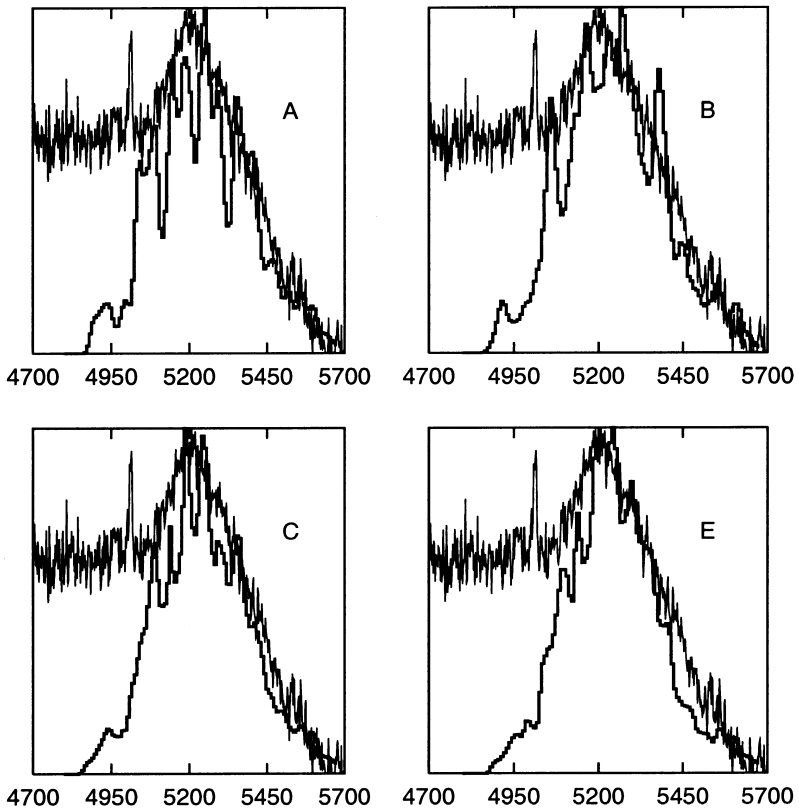

FIG. 6.—Profiles of the [Fe II] feature for hypernova models viewed at 5°; model A (*upper left panel*), model B (*upper right panel*), model C (*lower left panel*), and model E (*lower right panel*).

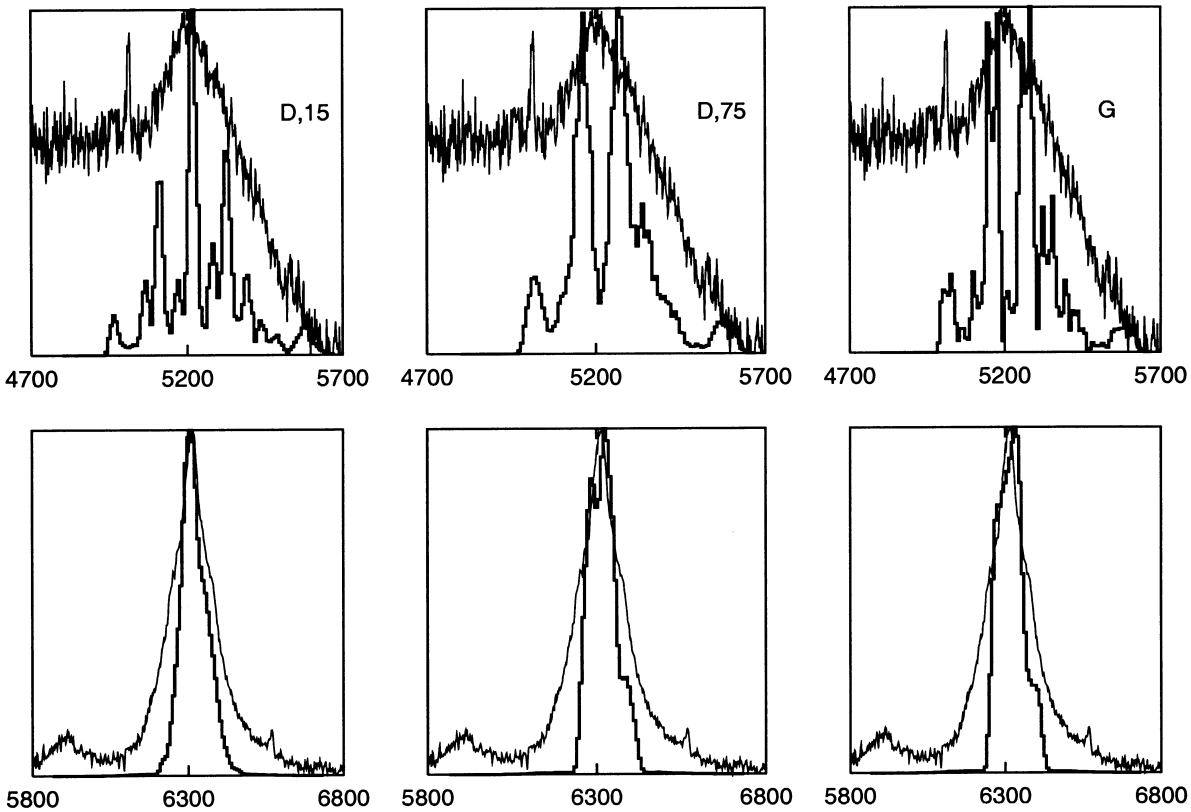

FIG. 7.—Profiles of the [Fe II] feature (*upper panels*) and the [O I] (*lower panels*) for normal energetic models. Those of model D viewed at 15° (*left panels*), 75° (*middle panels*), and model G (*right panels*) are shown.

~ 3000 km s^{-1} along the r-axis in this model. This corresponds to a Doppler shift of ~ 120 Å between the approaching and receding parts when the SN is viewed from the r-direction. Therefore, to produce the narrow and sharply peaked O line in a hypernova model, the explosion must be aspherical and viewed from near the polar direction.

Figure 6 shows the profiles of the [Fe II] blend viewed at 5° for various aspherical hypernova models (A, B, C, and E). In all of these models, the computed O line reproduces the observed one, as discussed above. The Fe blends appear to reproduce the 5200 Å feature reasonably well. The profiles shows small peaks, which are not seen in the observations. These peaks are more pronounced in more asymmetric models. Mixing of the ejecta may distribute the ^{56}Ni to lower velocities, thus reducing the double-peaked profiles of the Fe lines. A spherical hypernova model (model F; Fig. 4) also gives a broad Fe line, without the sharp peaks. However the O line is much too broad. Also, in this work we have used a spherical uniform-density nebular model to compute line emissivities. In an aspherical model, dense central and equatorial regions may have higher γ-ray trapping efficiency, which may result in stronger low-velocity line emission than in our model. Thus, the component iron lines in the blend may have wider, flat-topped profiles rather than double-peaked shapes, which could eliminate the minor peaks in the Fe blend seen in our present models. Two-dimensional γ-ray trapping calculations are therefore needed to compute the detailed spectra and the light curve.

It is reasonable to think that asphericity reduces the energy below that estimated previously based on spherically symmetric models. To examine this, we turn now to the lower energy explosion models (D, G). The [Fe II] and [O I] profiles for these models are shown in Figure 7. First of all, these models always give a narrower O line than that observed. In these low-energy models, in fact, the velocity of the ejecta is too small. The fastest moving matter approaches the observer with a velocity of 3500 km s^{-1} for model G and 5000 km s^{-1} in the case of the aspherical model (D) viewed from the z-direction. The observed FWHM (150 Å), however, indicates that there should be material moving faster than 7000 km s^{-1}. Also, because of the low velocity, the component [Fe II] lines are too narrow and do not blend to form a broad feature. From these arguments, we conclude that the explosion energy of SN 1998bw should have been large, $E_K \sim 1 \times 10^{52}$ ergs.

5. CONCLUSION AND DISCUSSION

We calculated the nucleosynthesis in aspherical hypernova explosions. We found that in such explosions Fe is mostly ejected at high velocity in a jet along the polar direction, while nearer the equatorial plane burning is less effective and low-velocity O is mostly ejected. We have shown that the unusual ratio of the width of the O and Fe nebular lines in SN 1998bw can be explained with a strongly aspherical explosion model viewed from a near-jet direction. Also, in this case the O line has a very sharp peak, in agreement with the observations.

Much of our discussion was based on the identification of the 5200 Å feature as a blend of [Fe II] lines. Although several caveats apply to that identification because other lines may contribute, we claim that [Fe II] lines dominate. Other possible contributions are as follows. According to Sollerman et al. (2000) the feature contains not only [Fe II] lines but also lines of [Mg I], [O I], and possibly [Fe I]. Lines of [Mg I] are included in our nebular code, and the strength of the 5172 Å emission, which is consistent with the 5470 Å line reproducing the observed [Mg I] peak near 4500 Å is much smaller than that of the [Fe II lines. [O I] 5577 Å is also included in our code and is strong and fills up the red part of the emission, but it does not contribute to the blue side (Mazzali et al. 2001). As for [Fe I], Sollerman et al. (2000) say that their models "have too low a degree of ionization," suggest that the density in the Fe-emitting regions should be lower, and "regard the Fe I emission as dubious." We confirm this result.

Another possibility is allowed Fe II emission, such as identified by Filippenko (1989) in the Type II SNe 1987F and 1988I and by Filippenko, Porter, & Sargent (1990) in the Type Ic SNe 1985F and 1987M. The main Fe II features are at 4570 Å (multiplets 37 and 38), 5190 Å (multiplet 42), and 5320 Å (multiplets 42 and 43). These lines are not included in our atomic model because not all the collision strengths for these transitions are available. In particular, multiplet 42 is not available. However, several arguments apply against the Fe II identification in SN 1998bw: (1) In SNe 1987F and 1988I all three features are strong, while in SNe 1985F and 1987M the feature at 4570 Å is narrow and is identified as [Mg I], suggesting that the feature at 5200 Å could be [Fe II]. A similar situation holds for SN 1998bw, also an SN Ic. (2) Fe II emission occurs at high density. Filippenko (1989) infers $\log n_e \sim 9$–10 for SN 1987F. However, the densities we derive for SN 1998bw are more than 1 order of magnitude smaller (Mazzali et al. 2001). (3) The relatively low density is confirmed by the large ratio (~ 4) of the Ca II IR emission compared to [Ca II] 7300 Å. Figure 2 of Ferland & Persson (1989) suggests that $\log n_e < 9$. Finally, the models of Mazzali et al. (2001), which are based on [Fe II] only, reproduce the 5200 Å feature very well. In any case, extending the model to include Fe II lines is a worthwhile effort that we intend to make.

The 5200 Å feature is bluer on November 26 and thereafter than on earlier epochs. Two principal factors are probably responsible for this: (1) the disappearance of the continuum, which is still significant in the earlier spectra, and (2) the reduced intensity of O I] 5577 Å, as shown in our models (Mazzali et al. 2001). This is a high-density line, and it decreases quickly in strength as the ejecta expand. Fading Fe II emission may also play a role in causing a small wavelength shift.

Weak unaccounted emission is present to the blue of the [Fe II] feature (4800–5100 Å). A similar emission is present in the nebular spectra of SNe Ia as well (Patat et al. 2001), and it is poorly reproduced by synthetic spectra. It may be due to a forest of weak [Fe II] and [CO I] transitions whose atomic parameters are not well known.

The [O I] line in other SNe Ib/c (Filippenko et al. 1995; Matheson et al. 2001) also shows a strongly peaked profile, as in SN 1998bw. This probably signals the existence of oxygen at low velocity in most SNe Ib/c. Although there are very few SNe Ib/c in which the feature centered at 5200 Å are detected with high enough signal to noise ratio, it appears that in these objects the [O I] line has a similar profile. For low-energy SNe (1×10^{51} ergs), the spherical model G shows a sharply peaked [O I] line profile (Fig. 7). This seems to favor spherical explosions for these low-energy SNe. However, it is premature to conclude that asymmetry is completely absent in low-energy SNe Ib/c because the effect of asphericity in a late-time spectra is not

so large in the case of normal SNe, as seen in Figure 7. This is due to the low expansion velocities. The oxygen line can be narrow even in the case of an aspherical explosion viewed from near the equator. For example, it is difficult to distinguish model D viewed from 75° from model G. Because the probability of viewing an aspherical SN from the near-polar direction is smaller than the probability of viewing one near the equator, the observations are not inconsistent with the possibility that most SNe Ib/c are more or less aspherical. More nebular spectra of SNe Ib/c with higher signal to noise ratio are needed for further investigation.

Our aspherical explosion models may be able to explain the slow decline of the late light curve of SN 1998bw. In these models, the equatorial region is denser than in a spherically symmetric model with the same explosion energy. At advanced epochs this region may be able to trap γ-rays more efficiently than a spherical model, as first suggested by Nakamura et al. (2001a). Chugai (2000) showed that a spherical model could reproduce the light curve if the density near the center (i.e., in the Fe-dominated region) was increased above that of the hydrodynamical model of Iwamoto et al. (1998). However, Sollerman et al. (2000) find that the O-dominated region should be dense and the Fe-dominated region not dense. Although taken individually these conclusions are probably correct, they appear to be in conflict with one another. An aspherical model offers a natural solution because it predicts the presence of high-density O-dominated matter near the center (Fig. 3).

A small degree of linear optical polarization ($\sim 0.5\%$) was reported in SN 1998bw (Kay et al. 1998; Iwamoto et al. 1998; Patat et al. 2001). This can be explained with different combinations of asphericity and viewing angle or with large-scale clumping in a basically spherical envelope. One solution is that ejecta with a moderate departure from sphericity are viewed from slightly off the axis of symmetry. Our strongly aspherical explosion model has an axis ratio of about 3 : 2 at the outer edge of the oxygen envelope (Fig. 3); therefore, it is consistent with the observed polarization if it is viewed from near the jet direction.

This work has been supported in part by the grant-in-aid for COE Scientific Research (07CE2002, 12640233) of the Ministry of Education, Science, Culture, and Sports in Japan.

REFERENCES

Axelrod, T. S. 1980, Ph.D. thesis, Lawrence Livermore Nat. Laboratory
Branch, D. 2001, in Supernovae and Gamma-Ray Bursts, ed. M. Livio et al. (Cambridge: Cambridge Univ. Press), 96
Chugai, N. N. 2000, Astron. Lett., 26, 797
Ferland, G. J., & Persson, S. E. 1989, ApJ, 347, 656
Filippenko, A. V. 1989, AJ, 97, 726
Filippenko, A. V., Porter A. C., & Sargent W. L. W. 1990, AJ, 100, 1575
Filippenko, A. V., et al. 1995, ApJ, 450, L11
Galama, T. J., et al. 1998, Nature, 395, 670
Hachisu, I., Matsuda, T., Nomoto, K., & Shigeyama, T. 1992, ApJ, 390, 230
———. 1994, A&AS, 104, 341
Iwamoto, K., et al. 1998, Nature, 395, 672
Kay, L. E., et al. 1998, IAU Circ., 6969
Khokhlov, A. M., Höflich, P. A., Oran, E. S., Wheeler, J. C., Wang, L., & Chtchelkanova, A. Yu. 1999, ApJ, 524, L107
MacFadyen, A. I., & Woosley, S. E. 1999, ApJ, 524, 262
Matheson, T., Filippenko, A. V., Leonard, D. C., & Shields, J. C. 2001, AJ, 121, 1648
Mazzali, P. A., Nomoto, K., Patat, F., & Maeda, K. 2001, ApJ, 559, 1047
Nagataki, S. 2000, ApJS, 127, 141
Nakamura, T., Mazzali, P. A., Nomoto, K., & Iwamoto, K. 2001a, ApJ, 550, 991
Nakamura, T., Umeda, H., Iwamoto, K., Nomoto, K., Hashimoto, M., Hix, R. W., & Thielemann, F.-K. 2001b, ApJ, 555, 880
Nomoto, K., & Hashimoto, M. 1988, Phys. Rep., 256, 173
Nomoto, K., et al. 2001a, in Supernovae and Gamma Ray Bursts, ed. M. Livio et al. (Cambridge: Cambridge Univ. Press), 144
Nomoto, K., et al. 2001b, in The Influence of Binaries on Stellar Population Studies, ed. D. Vanbeveren (Dordrecht: Kluwer), 507
Paczyński, B. 1998, ApJ, 494, L45
Patat, F., et al. 2001, ApJ, 555, 900
Sollerman, J., Kozma, C., Fransson, C., Leibundgut, B., Lundqvist, P., Ryde, F., & Woudt, P. 2000, ApJ, 537, L127
Thielemann, F.-K., Nomoto, K., & Hashimoto, M. 1996, ApJ, 460, 408
Woosley, S. E. 1993, ApJ, 405, 273
Woosley, S. E., Eastman, R. G., & Schmidt, B. P. 1999, ApJ, 516, 788